

Three-body break-up in deuteron-deuteron scattering at 65 MeV/nucleon

A. Ramazani-Moghaddam-Arani^{1,2,*}, H.R. Amir-Ahmadi², A.D. Bacher³, C.D. Bailey³,
 A. Biegun², M. Eslami-Kalantari^{2,4}, I. Gašparić⁵, L. Joulaeizadeh², N. Kalantar-Nayestanaki²,
 St. Kistryn⁶, A. Kozela⁷, H. Mardanpour², J.G. Messchendorp^{2,†}, A.M. Micherdzinska⁸,
 H. Moeini², S.V. Shende², E. Stephan⁹, E.J. Stephenson³, and R. Sworst⁶

¹ *Department of Physics, Faculty of Science, University of Kashan, Kashan, Iran*

² *KVI, University of Groningen, Groningen, The Netherlands*

³ *Center for Exploration of Energy and Matter, Indiana University, Bloomington, Indiana, USA*

⁴ *Department of Physics, Faculty of Science, Yazd University, Yazd, Iran*

⁵ *Rudjer Bošković Institute, Zagreb, Croatia*

⁶ *Institute of Physics, Jagiellonian University, Cracow, Poland*

⁷ *Henryk Niewodniczański, Institute of Nuclear Physics, Cracow, Poland*

⁸ *University of Winnipeg, Winnipeg, Canada and*

⁹ *Institute of Physics, University of Silesia, Katowice, Poland*

(Dated: November 10, 2018)

In an experiment with a 65 MeV/nucleon polarized deuteron beam on a liquid-deuterium target at KVI, several multi-body final states in deuteron-deuteron scattering were identified. For these measurements, a unique and advanced detection system, called BINA, was utilized. We demonstrate the feasibility of measuring vector and tensor polarization observables of the deuteron break-up reaction leading to a three-body final-state. The polarization observables were determined with high precision in a nearly background-free experiment. The analysis procedure and some results are presented.

PACS numbers: 21.30.-x, 24.70.+s, 25.45.De, 27.10.+h, 13.75.Cs, 13.85.-t

I. INTRODUCTION

The physics phenomena of nuclei are largely understood by considering the interaction between their building blocks, the nucleons. In 1935, Yukawa described the nucleon-nucleon (NN) force by the exchange of massive mesons [1] in analogy to the electromagnetic interaction which can be represented by the exchange of a massless photon. Several phenomenological nucleon-nucleon potentials have been derived based on Yukawa's theory and are able to reproduce data points in neutron-proton and proton-proton scattering with extremely high precision. These so-called high-quality NN potentials are used in Faddeev equations [2, 3] to give an exact solution of the scattering problem for the three-nucleon system. Already, for the simplest three-nucleon system, the triton, an exact solution of the three-nucleon Faddeev equations employing two-nucleon forces (2NFs) underestimates the experimental binding energy [4], showing that 2NFs are not sufficient to describe the three-nucleon system accurately. The existence of an additional force, the three-nucleon (3N) interaction, was predicted a long time ago by Primakov [5] and confirmed by a comparison between precision data and state-of-the-art calculations [6].

Many high-precision measurements of nucleon-deuteron scattering processes at intermediate energies

were carried out in the past decades with the aim to study 3NF effects and to compare the experimental observations with the predictions from rigorous Faddeev calculations. In general, adding 3NF effects to the modern NN potentials gives a better agreement between the cross section data for the proton-deuteron scattering processes and the corresponding calculations [7–17], whereas a similar comparison for the spin observables yields various discrepancies [9, 11, 13, 18–36]. The overall conclusion is that the spin-dependent parts of the 3NFs are poorly understood and that more studies in this field are needed.

The 3NF effects are in general small in the three-nucleon system. A complementary approach is to examine heavier systems for which the 3NF effects are significantly enhanced in magnitude. Naively, one might expect that the 3NF effects increase by the argument that the number of three-nucleon combinations with respect to two-nucleon combinations gets larger with increasing number of nucleons. We, however, note that the saturation of 3NF effects sets in very quickly for large nuclei as well. This simple counting rule is supported by a comparison between predictions and data for the binding energies of light nuclei [37]. The predictions of a Green's function Monte-Carlo calculation based on the Argonne V18 [38] NN interaction (AV18) and the Illinois-2 (IL2) 3NF [39] are compared to experimental data. While a calculation which only includes the AV18 NN potential deviates significantly from the experimental results, the predictions of calculations which include as well a 3NF come much closer to the data, especially for the first few

*Electronic address: ramazani@kvi.nl

†Electronic address: messchendorp@kvi.nl

light nuclei. Note that the effect of the 3NF on the binding energy for the triton is 0.5-0.8 MeV, whereas the effect increases significantly for the four-nucleon system, ${}^4\text{He}$, to ~ 4 MeV. For this, it was proposed to study the four-nucleon system at intermediate energies since the experimental database for this is presently poor in comparison with that of three-nucleon systems [40–43]. Most of the available data have been measured at very low energies, in particular below the three-body break-up threshold of 2.2 MeV. Also, theoretical developments are evolving rapidly at low energies [44–47], but lag behind at higher energies. This situation calls for extensive four-nucleon studies at intermediate energies.

This paper addresses the feasibility of measuring polarization observables in the three-body break-up channel in deuteron-deuteron scattering, $\vec{d} + d \rightarrow d + p + n$, for an incident beam energy of 65 MeV/nucleon. This work is part of a more extensive experimental program which was carried out at KVI and that aims to provide precision data in various four-nucleon scattering processes at intermediate energies. With these data, we will significantly enrich the four-nucleon scattering database at intermediate energies and, thereby, provide a basis to test future calculations with the long-term aim to understand the details of 3NF effects.

II. EXPERIMENT AND EXPERIMENTAL SETUP

Deuteron-deuteron scattering below the pion-production threshold leads to 5 possible final states with a pure hadronic signature, namely:

1. Elastic channel: $\vec{d} + d \rightarrow d + d$;
2. Neutron-transfer channel: $\vec{d} + d \rightarrow p + t$;
3. Proton-transfer channel: $\vec{d} + d \rightarrow n + {}^3\text{He}$;
4. Three-body final-state break-up: $\vec{d} + d \rightarrow p + n + d$;
5. Four-body final-state break-up: $\vec{d} + d \rightarrow p + n + p + n$.

The study and identification of these final states require an experimental setup with specific features, namely, a large phase space coverage, a good energy and angular resolution, and the ability for particle identification. The experiment presented in this paper was carried out at KVI using the Big Instrument for Nuclear-polarization Analysis, BINA, which meets all these requirements [34, 48]. This work is devoted to the three-body final state.

BINA is a setup with a nearly 4π geometrical acceptance and has been used in various few-nucleon scattering experiments to measure the scattering angles and energies of protons and deuterons with the possibility for particle identification. The detector is composed of a

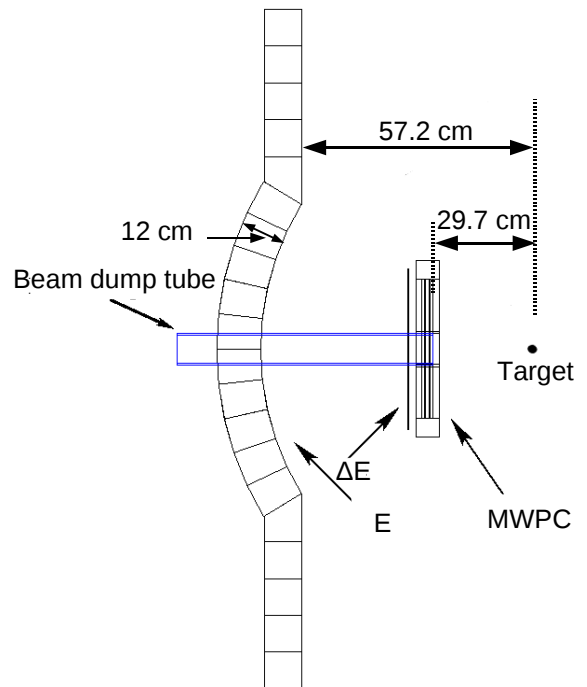


FIG. 1: (Color online) A side view of the forward part of BINA which consists of a Multi-Wire Proportional Chamber (MWPC), and an array of thin plastic scintillators ΔE , followed by a wall of thick segmented scintillators (E). The backward ball is not shown in this picture, since it was not used in the analysis presented in this paper.

forward part (forward wall) and a backward part. Figure 1 shows a side view of the forward part of BINA which consists of a Multi-Wire Proportional Chamber (MWPC), and an array of thin plastic scintillators (ΔE) with a thickness of 1 mm, followed by a wall of thick segmented scintillators (E) with a thickness of 12 cm each. All scintillators were read out by photo-multiplier tubes (PMTs) on both ends. The signals from these PMTs are integrated using a QDC to measure their energy loss in the scintillator. The discriminated signals from the Constant Fraction Discriminators (CFDs) are fed into Time-to-digital Converters (TDCs). The time difference between the signals from both ends of the scintillators allows to determine the position of the incoming particle. In addition, information about the time-of-flight (TOF)

of the particles can be extracted. The thick scintillators were mounted in a cylindrical shape, thereby, facing the target. The thickness of these scintillators is sufficient to stop all the protons and deuterons originating from the processes described in this work. The forward wall has a complete azimuthal coverage for scattering angles from 10° to 32° , which is advantageous for the determination of the beam polarization and spin observables. With the wire spacing of 2 mm and for a distance of 29.7 cm between MWPC and target, we obtain an overall accuracy of 0.4° for the polar angle and between 0.6° and 2.0° for the azimuthal angle. The detection efficiency of the MWPC was obtained by using an unbiased and nearly background-free data sample of elastically-scattered deuterons and was found to be typically 98% with an absolute uncertainty of 1%.

A polarized beam of deuterons originating from the polarized ion source (POLIS) [49] was accelerated by AGOR (Accélérateur Groningen ORsay) to a kinetic energy of 65 MeV/nucleon and bombarded on a liquid-deuterium target [50]. The polarization of the deuteron beam was measured in the low-energy beam line with a Lamb-Shift Polarimeter (LSP) [51] as well as in the high-energy beam line with BINA [48]. For the polarization measurements using the LSP, the low-energy beam was decelerated and focused on to the LSP detection system. The number of deuterons in the spin-up state, N_+ , spin-zero state, N_0 , and spin-down state, N_- , were counted to measure directly the vector and tensor polarizations of the beam. In addition, the polarization of the beam of deuterons was obtained at the high-energy beam line employing BINA via ϕ -asymmetry measurements of the ${}^1\text{H}(\vec{d}, dp)$ reaction based on its well-known analyzing power. Note that the same detector was used as well for the measurement of the polarization observables of the deuteron-deuteron break-up reaction. With the self-calibrating BINA setup, regular asymmetry measurements of the elastic deuteron-proton scattering process were performed during the actual experiment by switching rapidly the liquid target to a solid CH_2 target. The polarization of the beam of deuterons was studied as a function of time to check the stability of polarization during the measurement. Also, the polarization values by BINA were compared with those measured with the LSP. The results for the vector (top panel) and tensor (bottom panel) polarizations of the deuteron beam from BINA and LSP are shown in Fig. 2 as a function of time. Each filled circle represents the average value of the measured polarizations deduced from different scattering angles with BINA in a range from 55° to 140° in the center-of-mass frame. The corresponding analyzing powers were taken from an angle-dependent fit of literature values [15, 18, 33]. Polarization values obtained for different scattering angles were found to be in good agreement within uncertainties. The values of the polarization obtained with LSP are depicted as filled squares. The shaded bands represent the results of a constant-value fit through the data including the results obtained with BINA and LSP. The width

of the band corresponds to a 2σ error of the fit. The polarization values were found to be $p_Z = -0.57 \pm 0.03$ and $p_{ZZ} = -1.57 \pm 0.03$. The total uncertainties of the polarizations was estimated by adding quadratically the statistical error and the systematic error. The systematic uncertainty stems from the uncertainty in the analyzing powers, and was found to be 6% and 5% for the vector and tensor polarizations, respectively. A comparison between the results demonstrates that the beam polarization was stable during the experiments and that there is a good agreement between the measured values obtained at the low-energy beam line with the LSP and those measured at the high-energy beam line with BINA. The beam current was monitored during the experiments via a Faraday cup at the end of the beam line. The Faraday cup is made of a copper block containing a heavy alloy metal as the actual beam stopper. The current meter was connected to the Faraday cup with a short cable to avoid the voltage drop and pickup effect. The current meter was calibrated using a precision current source with an uncertainty of 2%. The beam current was typically 4 pA during the experiment. An offset of 0.24 ± 0.07 pA in the beam current was observed in the $\vec{d}d$ experiment through a comparison of T_{20} in elastic scattering, measured with BINA and the one measured with another experimental setup (BBS) [52].

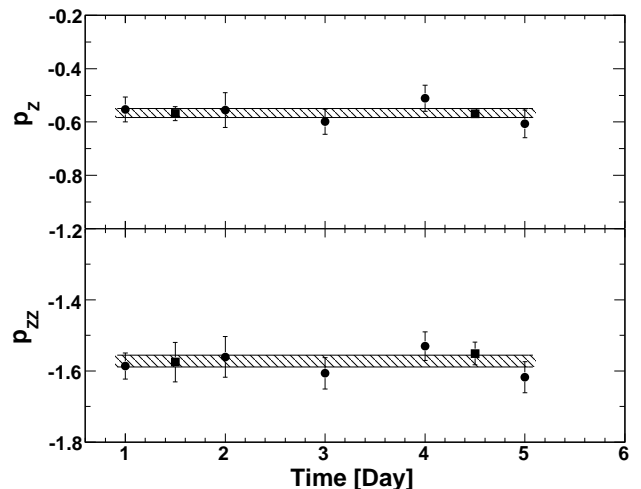


FIG. 2: The results for the vector (top panel) and tensor (bottom panel) polarizations of the deuteron beam. The filled circles and squares are the measured values by BINA and LSP, respectively. The shaded bands represent the result of a constant-value fit through all the data points.

III. ANALYSIS METHOD AND EVENT SELECTION

The elastic channel, neutron transfer channel, and break-up channels leading to three- and four-body final states were uniquely identified using the information on

the energies of the outgoing particles, their scattering angles, and their TOF. In this work, the deuteron-deuteron break-up into the three-body final-state (four-body final-state) is further referred to as the three-body break-up (four-body break-up). This is the first time that spin observables in the three-body break-up reaction in $\vec{d} + d$ scattering process at intermediate energies have been measured in a background-free experiment. The analysis procedure and a part of the results of the three-body break-up channel are presented in this paper.

The kinematics of the three-body break-up reaction are determined unambiguously by exploiting the scattering angles of the proton and the deuteron ($\theta_d, \theta_p, \phi_{12} = |\phi_d - \phi_p|$) and the relation between their energies presented by the kinematical curve which is referred to as the S -curve. The angles θ_p and θ_d are the polar angles of the proton and the deuteron, respectively, and ϕ_{12} is the difference between their azimuthal angles. The energies of the proton, E_p , and deuteron, E_d , were transferred into two new variables, D and S . The variable S is the arc-length along the S -curve with the starting point chosen arbitrarily at the point where E_d is minimum and D is the distance of the (E_p, E_d) point from the kinematical curve.

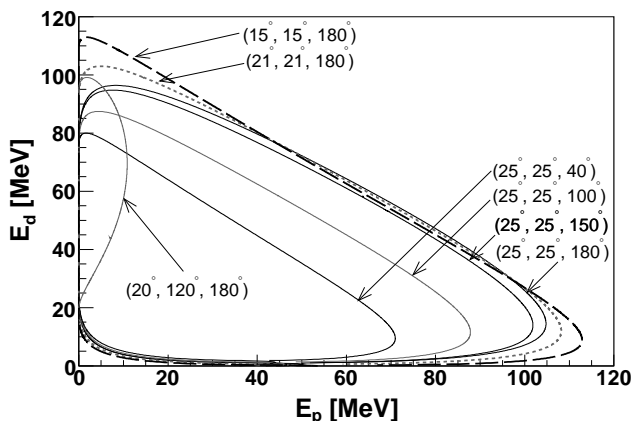


FIG. 3: The energy correlation between protons and deuterons in coincidence for the three-body break-up reaction in $\vec{d} + d$ scattering is shown as S -curves for several kinematical configurations. The kinematics are defined by $(\theta_d, \theta_p, \phi_{12})$, the polar scattering angles of the deuteron and proton, respectively, and their relative azimuthal angle.

The S -curves for several kinematical configurations are shown in Fig. 3. Each S -curve is labeled by three numbers. For example, the label $(20^\circ, 120^\circ, 180^\circ)$ shows a kinematical relation of energies of a deuteron that scatters to 20° and a proton that scatters to 120° , and the azimuthal opening angle, ϕ_{12} , between them is equal to 180° .

For the analysis of the three-body break-up data we measured the kinetic energies and the polar and azimuthal angles of the two coincident charged particles.

We performed the analysis of the three-body break-up reaction for that part of the phase-space in which the deuteron and the proton were detected in coincidence in the forward part of BINA.

For some parts of the ΔE detector, the yield of scintillation light reaching the photomultipliers was not sufficient to obtain a good particle identification. We, therefore, decided to make use of the time-of-flight to perform a particle identification instead. We note that the procedure was checked by a successful comparison with an analysis using those ΔE detectors which were operating according to specifications. For the particle identification, we measured the TOF of each registered particle and compared its result with the expectation from the kinematics of the three-body break-up reaction. The TOF was determined by discriminating the signals from the two PMTs from each scintillator. The output of the constant-fraction discriminators were fed into time-to-digital converters (TDCs) which were used in a common-stop mode. The common stop signal was derived from the radio frequency of the cyclotron. For the analysis of the break-up data, the TDC output corresponding to the left- and right-hand side PMTs, TOF_L and TOF_R , were added together for each event. The sum of TOF_L and TOF_R is independent of hit position along the scintillator slab. We call this sum TOF_i with i referring to the different particles that hit the forward wall. For particle identification, we compared these results with the expected TOF that was calculated from the energy of a particle, calculating a path length from a scattering angle and assuming a certain particle type. More precisely, the difference between the measured TOF of particles 1 and 2 from the information of the TDCs, $(\text{TOF}_1 - \text{TOF}_2)_{\text{TDC}}$, and that extracted from the energies and the scattering angles, $(\text{TOF}_1 - \text{TOF}_2)_E$, has been used to define the variable ΔTOF . We note that ΔTOF is a difference of differences, and that it compares data with a kinematics calculations, both of which yield a difference. The identification of the break-up channels proceeds by analyzing ΔTOF .

Figure 4 shows the value of ΔTOF for two particles that are detected in coincidence in the forward wall. The scattering angle of both particles is fixed to be $25^\circ \pm 2^\circ$ and the difference between the azimuthal angles of the two particles is $180^\circ \pm 5^\circ$. We note that ΔTOF does not depend upon S and that the detected particle in each hit can be a proton or a deuteron. Three clear peaks can be recognized corresponding to proton-deuteron, proton-proton, and deuteron-proton coincidences. The identification of the peaks were confirmed using the ΔE responses. For this spectrum, we assumed in the calculation of $(\text{TOF}_1 - \text{TOF}_2)_E$ that the first particle is a deuteron and the second one a proton. If our assumption is correct, events which correspond to a deuteron-proton combination will give a peak around zero in the ΔTOF spectrum. Note that a clear signal (peak on the left-hand side of Fig. 4) of the three-body break-up events can be observed corresponding to a final-state consist-

ing of a deuteron-proton combination. The peak on the most right-hand side corresponds to three-body break-up events, but with a proton-deuteron combination in the final state. The peak in the middle of the spectrum has been identified as two protons that stem from the four-body break-up reaction.

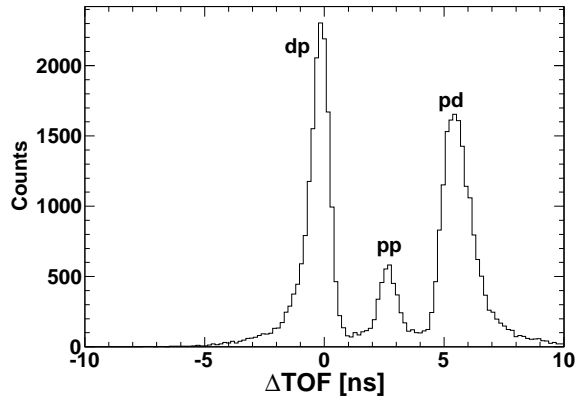


FIG. 4: The measured ΔTOF for two particles that are detected in coincidence in the forward wall. The scattering angle of both particles is fixed to be $25^\circ \pm 2^\circ$ and the difference between the azimuthal angles of the two particles is $180^\circ \pm 5^\circ$.

The top-left panel of Fig. 5 represents the correlation between the energy of two particles that are detected in coincidence in the forward wall. The scattering angle of both particles is fixed to be $25^\circ \pm 2^\circ$ and the difference between the azimuthal angles of the two particles is $180^\circ \pm 5^\circ$. The energies were obtained by a charge-integration of the signals from the PMTs of the forward scintillators. This spectrum contains events from two different reactions, namely three- and four-body break-up reactions. The proton-deuteron or deuteron-proton coincidences from the three-body break-up reaction can be separated by choosing events corresponding to the peak of interest as shown in Fig. 4. The results are shown in the top-right and bottom-right panels. The bottom-left panel contains events which correspond to the peak in the middle of Fig. 4. They originate from the four-body break-up channel. Figures 4 and 5 demonstrate the particle identification capabilities of the detection system.

The identification of the proton and deuteron enables us to measure the missing particle in the three-body break-up reaction in deuteron-deuteron scattering. The missing particle in this reaction is neutron as well. This particle can be identified using the missing mass technique. We used the energy and scattering angles of the identified particles to calculate the rest mass of the undetected particle. Figure 6 shows a typical result of the calculated mass of the undetected particle using the energy, polar and azimuthal angles of the detected proton and deuteron. The scattering angle of both detected particles is fixed to be $25^\circ \pm 2^\circ$ and the difference between the azimuthal angles of the two detected particles

is $180^\circ \pm 5^\circ$. The dashed (solid) curve represents the results of the calculated missing particle mass before (after) applying the identification cut on Fig. 4. After applying the identification cut the mass spectra show a clear peak corresponding to the mass of neutrons with a FWHM of 6.38 MeV which confirms the accuracy of PID procedure. The events on the right-hand side of the peak correspond to break-up events that undergo a hadronic interaction in the scintillator. These are discarded in the analysis and properly accounted for in the final analysis of cross sections with the help of simulations.

The next step in the event selection for the three-body break-up channel is to find the energy correlation between the final-state protons and deuterons for a particular kinematical configuration $(\theta_d, \theta_p, \phi_{12})$. The number of break-up events in an interval $S - \frac{\Delta S}{2}$, and $S + \frac{\Delta S}{2}$ was obtained by projecting the events on a line perpendicular to the S -curve (D -axis). The value of ΔS was ± 5 MeV for the forward wall data. Figure 7 depicts the correlation between the energy of protons and deuterons in coincidence for the kinematical configuration, $(\theta_d, \theta_p, \phi_{12}) = (25^\circ, 25^\circ, 180^\circ)$. The solid curve is the expected correlation for this configuration. One of the many S -intervals and the corresponding D -axis are also shown. The result of the projection of events on the D -axis for a particular S -bin is presented in the inset of Fig. 7. This spectrum consists of mainly break-up events with a negligible amount of accidental background. Most of the particles of the break-up events deposit all their energy in the scintillator, which gives rise to a peak around zero in the variable D . The events on the left-hand side of the peak at zero correspond to break-up events that undergo a hadronic interaction in the scintillator (same as those on the right side of the peak in Fig. 6).

The interaction of a polarized beam with an unpolarized target produces an azimuthal asymmetry or an azimuthally uniform change in the scattering cross section. The magnitude of this effect is proportional to the product of the polarization of the beam and an observable that is called the analyzing power. The expression for the cross section of any reaction induced by a polarized spin-1 projectile is [53, 54]:

$$\begin{aligned} \sigma(\xi, \phi) = \sigma_0(\xi) & \left[1 + \sqrt{3} p_Z \text{Re}(iT_{11}(\xi)) \cos \phi \right. \\ & - \frac{1}{\sqrt{8}} p_{ZZ} \text{Re}(T_{20}(\xi)) \\ & \left. - \frac{\sqrt{3}}{2} p_{ZZ} \text{Re}(T_{22}(\xi)) \cos 2\phi \right], \quad (1) \end{aligned}$$

where σ and σ_0 are the polarized and unpolarized cross sections, respectively, and ξ represents the configuration $(\theta_d, \theta_p, \phi_{12}, S)$. Note that Eq. 1 does not contain terms with $\text{Im}(iT_{11})$, $\text{Re}(T_{21})$, $\text{Im}(T_{21})$, $\text{Im}(T_{20})$ and $\text{Im}(T_{22})$. These contributions vanish because we took explicitly $\beta = 90^\circ$ and ϕ_{12} is the absolute value of the difference between the azimuthal angles of the two outgoing particles. The angle β is the angle between the polarization axis and the momentum of the incoming beam. In this

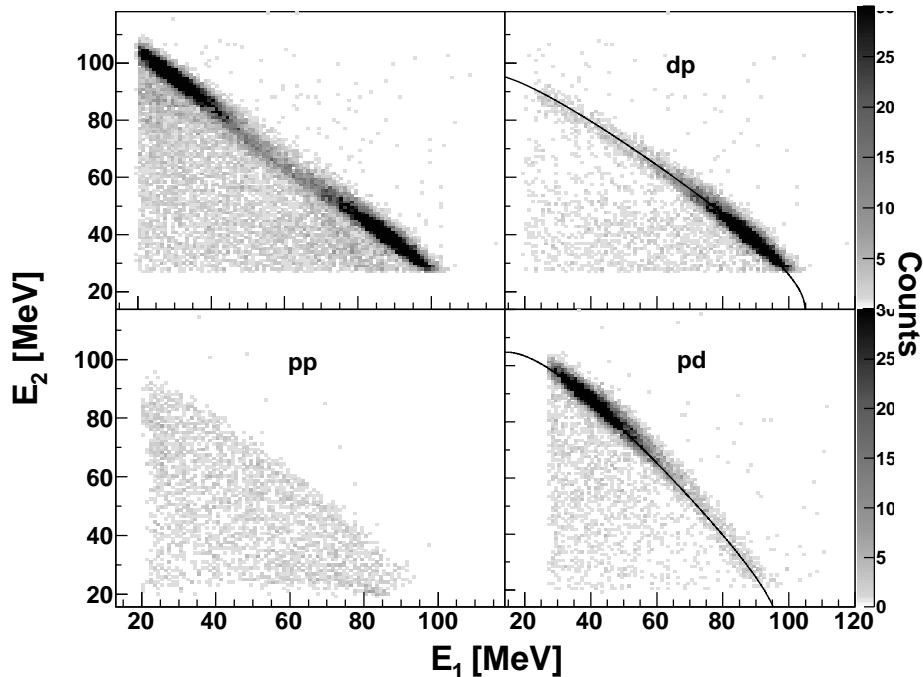


FIG. 5: The correlation between the calibrated energy of the two outgoing particles (proton or deuteron) in the deuteron-deuteron break-up process is shown for the coplanar configuration, $(\theta_1, \theta_2, \phi_{12}) = (25^\circ, 25^\circ, 180^\circ)$ before PID (top left panel) and after PID (other panels). The bottom-panel on the left-hand side depicts events from the four-body break-up reaction and the two panels on the right-hand side correspond to the three-body break-up channels. The solid curves represent the relativistic S -curve that are calculated from the energy and momentum conservation for the selected configuration.

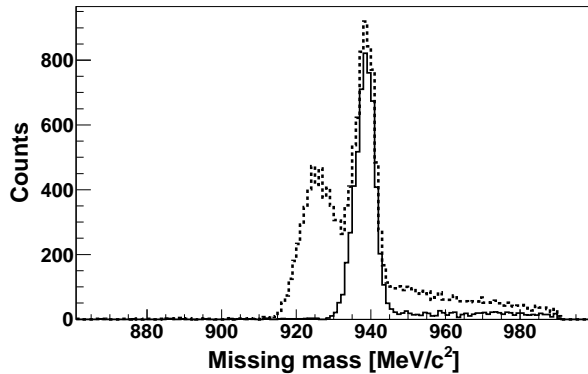


FIG. 6: The calculated mass of the undetected particle in the three-body break-up reaction in deuteron-deuteron scattering. The energy, polar and azimuthal angles of the detected protons are used in the calculation. The dashed (solid) curve represents value of the calculated mass of the missing particle before (after) applying the identification cut in Fig. 4. The scattering angle of both detected particles is fixed to be $25^\circ \pm 2^\circ$ and the difference between the azimuthal angles of the two detected particles is $180^\circ \pm 5^\circ$.

work, the variables $\text{Re}(iT_{11})$, $\text{Re}(T_{20})$ and $\text{Re}(T_{22})$ will be referred to as iT_{11} , T_{20} and T_{22} , respectively. The

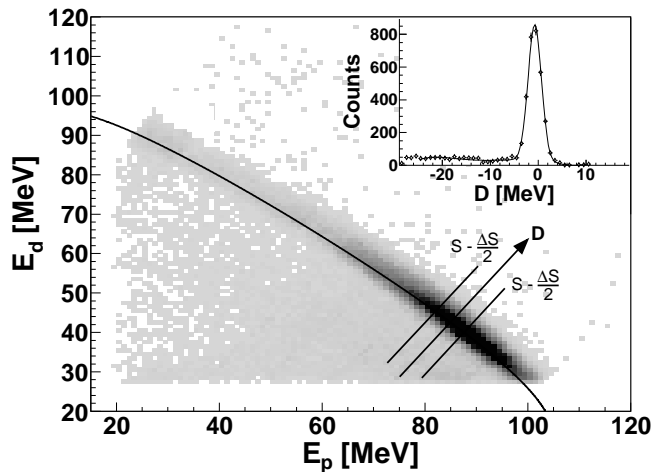


FIG. 7: The correlation between the energies of the deuteron and the proton originating from the three-body break-up channel in one selected configuration. The projection of the events from one S -bin onto the D -axis is shown in the inset.

quantities iT_{11} and p_Z are the vector-analyzing power and the vector beam polarization, respectively. The observables T_{20} and T_{22} are the tensor-analyzing powers, p_{ZZ} is the tensor polarization of the beam, and ϕ is the

azimuthal scattering angle of the deuteron.

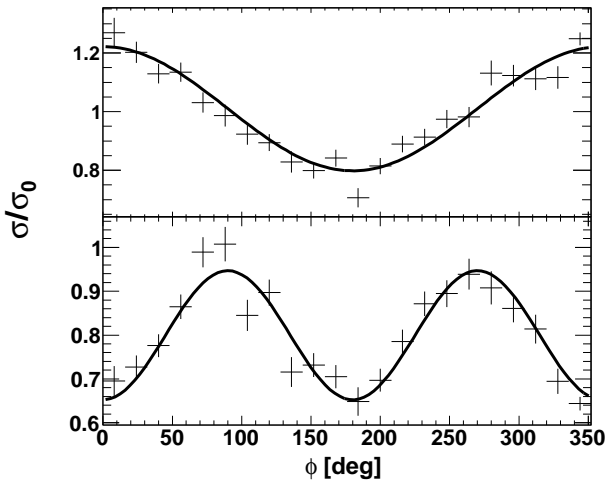


FIG. 8: The ratio of the spin-dependent cross section to the unpolarized one for a pure vector-polarized deuteron beam (top panel) and a pure tensor-polarized deuteron beam (bottom panel) for $(\theta_d = 25^\circ, \theta_p = 25^\circ, \phi_{12} = 180^\circ, S = 230 \text{ MeV})$.

For a deuteron beam with a pure vector polarization, the ratio $\frac{\sigma}{\sigma_0}$ should show a $\cos\phi$ distribution where σ and σ_0 are the polarized and unpolarized cross sections, respectively. When a pure tensor-polarized deuteron beam is used, the ratio $\frac{\sigma}{\sigma_0}$ should show a $\cos 2\phi$ distribution. These asymmetries are exploited to extract the vector-analyzing power, iT_{11} and the tensor-analyzing powers, T_{20} and T_{22} , for every kinematical configuration, $(\theta_d, \theta_p, \phi_{12}, S)$.

IV. EXPERIMENTAL RESULTS

For a measurement of the analyzing powers, we compare the distribution of the scattered particles at different azimuthal angles for each polarization state with that obtained with the unpolarized beam. The ϕ -distribution obtained with the polarized beam is normalized to that obtained with an unpolarized beam to obtain the ratio $\frac{\sigma}{\sigma_0}$. This ratio depends on the the number of counts under the peak after background subtraction and the total integrated charge collected in the Faraday cup. With this normalization other parameters like the geometrical asymmetries, inefficiencies, and target thickness are eliminated. Figure 8 shows the ratio $\frac{\sigma}{\sigma_0}$ for a pure vector-polarized deuteron beam (top panel) and a pure tensor-polarized deuteron beam (bottom panel) for $(\theta_p = 25^\circ, \theta_d = 25^\circ, \phi_{12} = 180^\circ, S = 230 \text{ MeV})$. The curves in the top and bottom panels are the results of a fit based on Eq. 1 through the obtained asymmetry distribution for a beam with a pure vector and tensor polarization, respectively. The amplitude of the $\cos\phi$ modulation in the top panel equals to $\sqrt{3}p_{ZZ}iT_{11}$ and that of the $\cos 2\phi$ mod-

ulation in the lower panel equals to $-\frac{\sqrt{3}}{2}p_{ZZ}T_{22}$. The offset from 1 in the lower panel is $-\frac{1}{\sqrt{8}}p_{ZZ}T_{20}$. The vector- and tensor-analyzing powers for a few kinematical configurations of the three-body break-up reaction were extracted. Figure 9 represents the vector- and tensor-analyzing powers at $(\theta_d, \theta_p) = (15^\circ, 15^\circ)$ (open squares) and $(\theta_d, \theta_p) = (25^\circ, 25^\circ)$ (filled circles) as a function of S for different azimuthal opening angles. The gray lines in all panels show the zero level of the analyzing powers. Only statistical uncertainties are indicated. The total systematic uncertainty for the analyzing power is estimated to be $\sim 7.5\%$ which mainly stems from the uncertainty in the measurement of the beam polarization via elastic scattering and to a much lesser extent from the error of the beam-current correction in the analysis of the T20 in the elastic d + d channel.

This paper demonstrates for the first time the feasibility of obtaining precision data of the three-body break-up channel in deuteron-deuteron scattering at the energy of 65 MeV/nucleon. The three-body break-up reaction has been clearly identified using the measured scattering angles, energies, and TOF of the final-state protons and deuterons. In this work, we analyzed a part of the data in which the protons and deuterons were scattered into the forward wall of BINA. We have provided precision data for the vector and tensor analyzing powers of the three-body break-up reaction for an incident deuteron beam of 65 MeV/nucleon [48]. These four-body scattering experiments at KVI will provide in the near future a complete database in deuteron-deuteron scattering at intermediate energies including the elastic, transfer, three-body break-up, and four-body break-up channels. Together with the upcoming state-of-the-art ab-initio calculations [55–57], these data will provide the basis to understand the mechanisms behind many-body force effects.

V. ACKNOWLEDGMENTS

The authors acknowledge the work by the cyclotron and ion-source groups at KVI for delivering a high-quality beam used in these measurements. This work was performed as part of the research program of the “Stichting voor Fundamenteel Onderzoek der Materie” (FOM). Furthermore, the present work has been performed with financial support from the University of Groningen (RuG), the Helmholtzzentrum für Schwerionenforschung GmbH (GSI), Darmstadt, the Nederlandse Organisatie voor Wetenschappelijk Onderzoek (NWO), the Polish 2008-2011 science funds as a research project No. N N202 078135 and Iran Ministry of Science, Research, and Technology, Kashan university. CDB and EJS acknowledge support from the US National Science Foundation through grant PHY 04-57219.

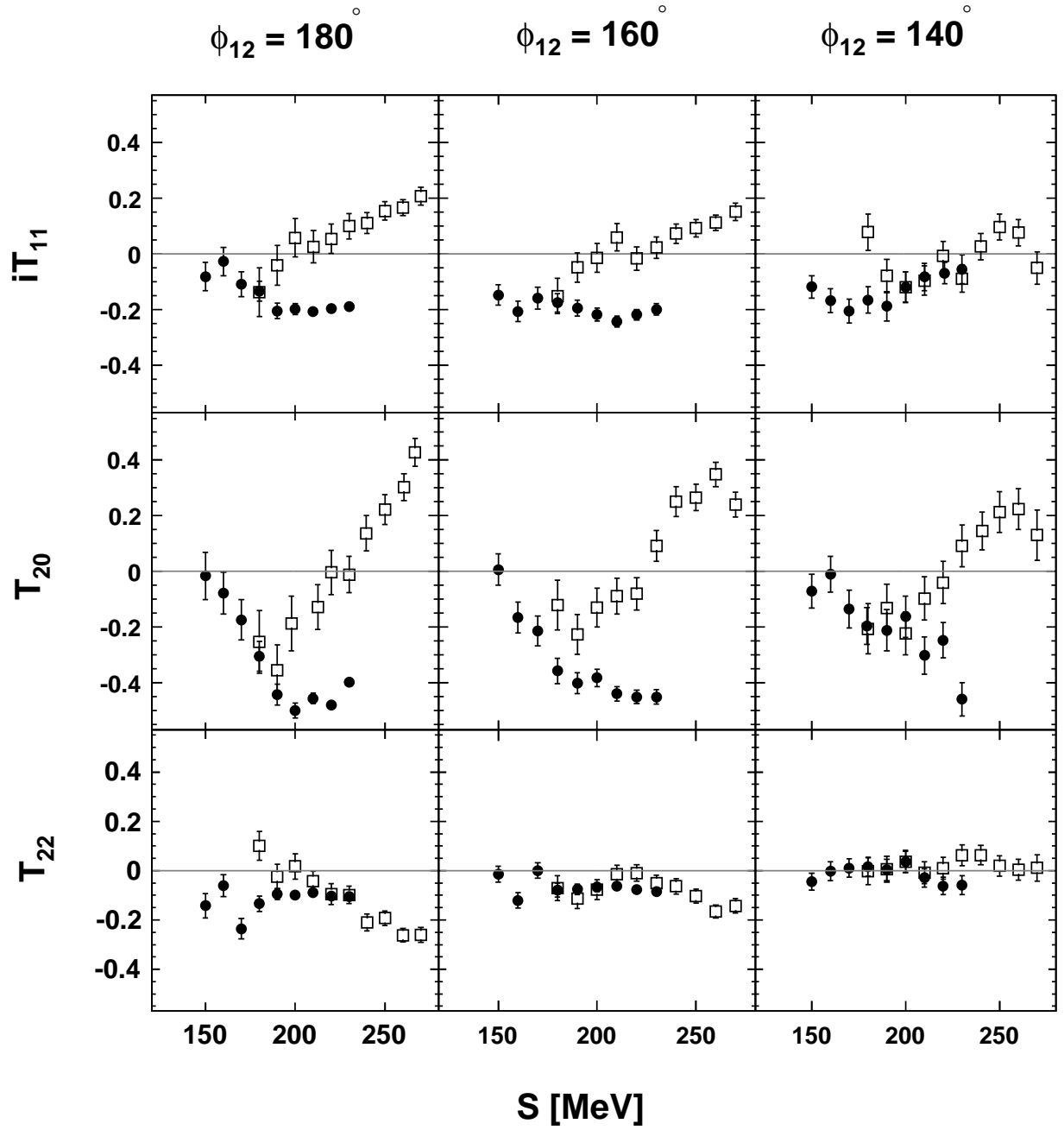


FIG. 9: The vector- and tensor-analyzing powers at $(\theta_d, \theta_p) = (15^\circ, 15^\circ)$ (open squares) and $(\theta_d, \theta_p) = (25^\circ, 25^\circ)$ (filled circles) as a function of S for different azimuthal opening angles. The gray lines in all panels show the zero level of the analyzing powers. Only statistical uncertainties are indicated.

-
- [1] H. Yukawa, Proc. Phys. Math. Soc. Jap. **17**, 48 (1935).
 [2] L. D. Faddeev, Sov. Phys. JETP. **12**, 1014 (1961).
 [3] W. Glöckle, H. Witała, D. Hüber, H. Kamada and J. Golak, Physics Reports **274**, 107 (1996).
 [4] R. B. Wiringa, A. R. Smith, and T. L. Ainsworth, Phys. Rev. C. **29**, 1207 (1984).
 [5] H. Primakoff, and T. Holstein, Phys. Rev. **55**, 1218 (1939).
 [6] H. Witała, W. Glöckle, D. Hüber, J. Golak and H. Kamada Phys. Rev. Lett. **81**, 1183 (1998).
 [7] H. Shimizu *et al.*, Nucl. Phys. A **382**, 242 (1982).
 [8] H. Sakai *et al.*, Phys. Rev. Lett. **84**, 5288 (2000).

- [9] K. Ermisch *et al.*, Phys. Rev. Lett. **86**, 5862 (2001).
- [10] K. Ermisch *et al.*, Phys. Rev. C **68**, 051001 (2003).
- [11] H. Hatanaka *et al.*, Eur. Phys. J. A **18**, 293 (2003).
- [12] E. Stephan *et al.*, Phys. Rev. C **76**, 057001 (2005).
- [13] K. Ermisch *et al.*, Phys. Rev. C **71**, 064004 (2005).
- [14] K. Sekiguchi *et al.*, Phys. Rev. Lett. **95**, 162301 (2005).
- [15] H. Mardanpour *et al.*, Eur. Phys. J. A **31**, 383 (2007).
- [16] A. Ramazani-Moghaddam-Arani *et al.*, Few-body system **44**, 27 (2008).
- [17] A. Ramazani-Moghaddam-Arani *et al.*, Phys. Rev. C **78**, 014006 (2008).
- [18] H. Witała, T. Gornelius and W. Glöckle, Few-body system **15**, 67 (1993).
- [19] E. J. Stephenson, H. Witała, W. Glöckle, H. Kamada, and A. Nogga Phys. Rev. C **60**, 061001(R) (1999).
- [20] J. G. Messchendorp *et al.*, Phys. Lett. B **481**, 171 (2000).
- [21] R. Bieber *et al.*, Phys. Rev. Lett. **84**, 606 (2000).
- [22] R. V. Cadman *et al.*, Phys. Rev. Lett. **86**, 967 (2001).
- [23] J. Kuroś-Żołnierczuk, *et al.*, Phys. Rev. C **66**, 024003 (2002).
- [24] K. Sekiguchi *et al.*, Phys. Rev. C **65**, 034003 (2002).
- [25] K. Hatanaka *et al.*, Phys. Rev. C **66**, 044002 (2003).
- [26] H. O. Meyer *et al.*, Phys. Rev. Lett. **93**, 112502 (2004).
- [27] K. Sekiguchi *et al.*, Phys. Rev. C **70**, 014001 (2004).
- [28] A.A. Mehmandoost-Khajeh-Dad *et al.*, Phys. Lett. B **617**, 18 (2005).
- [29] B. v. Przewoski *et al.*, Phys. Rev. C **74**, 064003 (2006).
- [30] S. Kistryn *et al.*, Phys. Lett. B **641**, 23 (2006).
- [31] A. Biegun *et al.*, Acta Phys. Pol. B **371**, 213 (2006).
- [32] H. Amir-Ahmadi *et al.*, Phys. Rev. C **75**, 041001 (2007).
- [33] E. Stephan *et al.*, Phys. Rev. C **76**, 057001 (2007).
- [34] H. Mardanpour, Ph.D. thesis, University of Groningen (2008).
- [35] M. Eslami-Kalantari, Ph.D. thesis, University of Groningen (2009).
- [36] H. Mardanpour *et al.*, Phys. Lett. B **687**, 149 (2010).
- [37] S. C. Pieper, V. R. Pandharipande, R. B. Wiringa, and J. Carlson, Phys. Rev. C **64**, 014001 (2001).
- [38] R. B. Wiringa, V. G. J. Stoks, and R. Schiavilla, Phys. Rev. C **51**, 38 (1995).
- [39] B. S. Pudliner, V. R. Pandharipande, J. Carlson, and R. B. Wiringa, Phys. Rev. Lett. **74**, 4396 (1995).
- [40] V. Bechtold, L. Friedrich, M. S. Abdel-Wahab, J. Bialy, M. Junge, and F. K. Schmidt, Nucl. Phys. A **288**, 189 (1977).
- [41] C. Alderliesten, A. Djaloeis, J. Bojowald, C. Mayer-Böricke, G. Paic, and T. Sawada, Phys. Rev. C **18**, 2001 (1978).
- [42] M. Garçon *et al.*, Nucl. Phys. A **458**, 287 (1986).
- [43] A. M. Micherdzińska, *et al.*, Phys. Rev. C **75**, 054001 (2007).
- [44] F. Ciesielski and J. Carbonell and C. Gignoux, Phys. Lett. B **447**, 199 (1999).
- [45] A. C. Fonseca, Phys. Rev. Lett. **83**, 4021 (1999).
- [46] M. Viviani, A. Kievsky, S. Rosati, E. A. George, and L. D. Knutson, Phys. Rev. Lett. **86**, 3739 (2001).
- [47] R. Lazauskas, J. Carbonell, A. C. Fonseca, M. Viviani, A. Kievsky, and S. Rosati, Phys. Rev. C **71**, 034004 (2005).
- [48] A. Ramazani-Moghaddam-Arani, Ph.D. thesis, University of Groningen (2009).
- [49] H. R. Kremers and A. G. Drentje, Vol. 421 of AIP Conf. Proc., edited by R. J. Holt and M. A. Miller (AIP, New York, 1997), p. 507.
- [50] N. Kalantar-Nayestanaki, J. Mulder and J. Zijlstra, Nucl. Instr. and Meth. in Phys. Res. A **417**, 215 (1998).
- [51] H. R. Kremers, J.P.M. Beijers, N. Kalantar-Nayestanaki, and T.B. Clegg, Nucl. Instr. and Meth. in Phys. Res. A **516**, 209 (2004).
- [52] A. M. van den Berg, Nucl. Instr. and Meth. in Phys. Res. B **99**, 637 (1995).
- [53] G. G. Ohlsen, Rep. Prog. Phys. **35**, 717 (1972).
- [54] G. G. Ohlsen, Nucl. Instr. Meth. **179**, 283 (1981).
- [55] A. Deltuva, and A. C. Fonseca, Phys. Rev. C **76**, 021001(R) (2007).
- [56] A. Deltuva, and A. C. Fonseca, Phys. Rev. C **75**, 014005 (2007).
- [57] A. Deltuva, Private communication.

